

Root Cause Failure Analysis of Pinch Roll Bearing at Hot Strip Mill

Kaushal Kishore · Goutam Mukhopadhyay

Submitted: 28 April 2018 / in revised form: 9 November 2018 / Published online: 24 January 2019
© ASM International 2019

Abstract Bearings are one of the most widely used and highly stressed engineering components. If properly manufactured, mounted, operated and maintained, they can give excellent service life. However, they may suffer from premature failure due to multitudes of reasons. Current work deals with pinpointing failure mode and root cause analysis of a pinch roll bearing at coil box of a Hot Strip Mill. Macroscopic and microscopic analysis revealed that bearing failed in Rolling Contact Fatigue mode. All metallurgical, mechanical and maintenance factors that might contribute to rolling contact fatigue were analyzed independently. It was concluded that misalignment led to accelerated Rolling Contact Fatigue. Striation marks rarely reported for rolling contact fatigue of bearing steels were observed to confirm fatigue mode of failure. Recommendations for preventing similar failures in future have been provided.

Keywords Pinch roll bearing · Rolling contact fatigue · Misalignment · Fatigue striations

Introduction

Bearings are used in engineering applications to transfer axial, radial or combined radial and axial loads [1]. These are available in a vast range of sizes, from a few millimeter size used in ceiling fans and motorbikes to over a few meters used in heavy engineering applications such as shoveling dozers. In each case, bearings are used to serve a particular function; and based on the applied load, speed of

the rotating element (s), operating temperature, and design and process safety factors, selection of bearing material and lubricants is made. If bearings are properly selected, mounted, operated and maintained, they can give excellent service life.

Over the past few decades, steel making processes have seen significant improvement to closely control the chemistry. Special efforts have been made to keep sulfur, phosphorus and oxygen to as low level as possible. External desulphurization has helped a long way in achieving the desired levels of sulfur. On the other hand, advances in vacuum treatments have made it possible to reduce oxygen to low levels. These efforts have manifested as a marked improvement in fatigue life of bearing elements by minimizing the presence of deleterious oxide and sulfide inclusions. Similarly, breakthroughs have been made in the field of operating practices, maintenance and in optimum quality and frequency of lubrication by a combination of analytic models and field expertise. However, despite these improvements, bearing failures are encountered and their failures are a bottleneck in uninterrupted operation. Common causes of bearing failures can be broadly classified into manufacturing, operational and maintenance-related issues [2–6]. Manufacturing-related issues can be (1) inferior chemistry, (2) presence of severe nonmetallic inclusions, (3) improper heat treatment that can result in lower hardness. Likewise, operational and maintenance factors that may contribute to failures of bearings include (1) overloading, (2) improper lubrication, (3) excessive vibration, (4) contamination, (5) presence of corrosive environment or fluid, (6) improper fitting and (7) misalignment.

Current work is focused on determining the failure mode and root cause of a pinch roll bearing that failed

K. Kishore (✉) · G. Mukhopadhyay
R&D and Scientific Services, Tata Steel, Jamshedpur, India
e-mail: kaushal.kishore3@tatasteel.com

prematurely during its service by considering each of these factors using detailed macroscopic and microscopic analysis at different length scales. This pinch roll bearing was installed at coil box of a hot strip mill. Its failure led to interruption in regular production with significant financial implications. Detailed analysis and corrective actions can prevent such failures in future.

Process Flow and On-Site Observations

Figure 1 shows process flow of a hot strip mill where slabs from the caster are converted into hot-rolled sheets. Slabs received from slab yards are reheated to a temperature above the recrystallization temperature in a reheating furnace flushed with argon gas to render it suitable for hot rolling. Despite the presence of inert argon gas, surface scales form on the slabs; and this is removed in a slab descaler where water jets at a pressure of around 170 bar impinge on the surface of the slab and remove the scale by the virtue of its high pressure. The slab passes through a set of rolls, and a vertical edger is placed to control the width of the slab, which remains virtually constant during the entire rolling process. For this very reason, rolling is referred as a plane strain process in which decrease in thickness is accompanied by proportionate increase in length of the work piece to keep the volume constant. The slab passes through a reversing roughing mill where primary reduction in thickness takes place. The reversing mill is a four high mill with two work rolls and two back up rolls to support them. Here, the slab moves to and fro 6–7 times and reduction takes place in each pass. Thereafter, traversing through a set of rolls, it reaches the coil box which acts as a buffer and maintains the continuity of the entire process. In addition, during the coiling stage, homogeneity of coil temperature takes place. It is at this

particular location where the failed pinch roll bearing was located. Its function was to drive the rollers. Due to the failure, there was an interruption in production. Beyond the coil box, sheets are uncoiled for subsequent reduction and phase transformations. At crop-shear, sheets are cut to predetermined programmed lengths. It goes through a secondary de-scaler to remove any scale that developed during the rolling process. This is followed by final thickness reduction in 4 high, 6 stand finishing mill. After attaining the desired reduction in thickness, steel sheets pass through a set of rolls and are subjected to laminar cooling. Here, water flow rate is controlled to attain the desired cooling rate and phase transformation. It then goes to the down coiler, and the finish rolling temperature (FRT) determines the final microstructure in the hot-rolled product.

Figure 2a shows the schematic of the overall arrangement of rolls in hot strip mill. There are a number of rolls with specific functions. There are bend rolls, deflector rolls and entry rolls, and all of these fundamentally allow the workpiece to enter the forming roll in the desired alignment where reduction in thickness takes place. There are two sets of cradle rolls used for coiling of the steel sheets. Uncoiling takes place with the help of pinch rolls. There are top pinch rolls and bottom pinch rolls, and they work in conjunction to maintain the continuity of the hot rolling process as shown in Fig. 2b. These are driven by a motor-connected bearing assembly. Failure occurred in the bottom entry pinch roll in its drive side as shown in Fig. 2c.

The bearing was found to be jammed and broken into multiple pieces. It failed after 5 months of service as against an expected life of at least 1 year. This reduction in service to less than half of its expected life is the motivation behind an in-depth failure analysis to understand its root cause and take corrective actions to prevent such failures in the future.

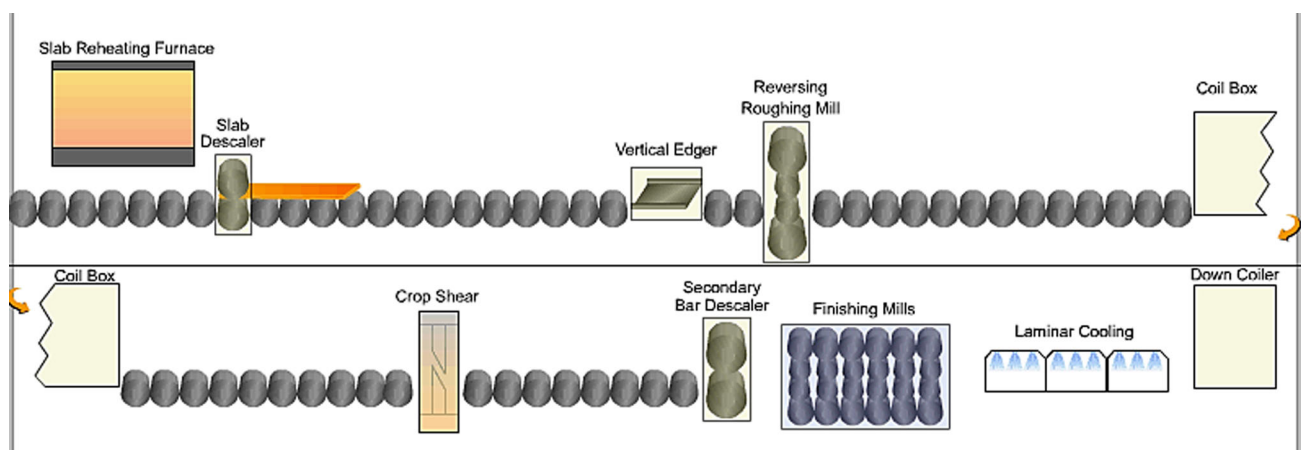


Fig. 1 Schematic of hot strip mill showing overall process flow

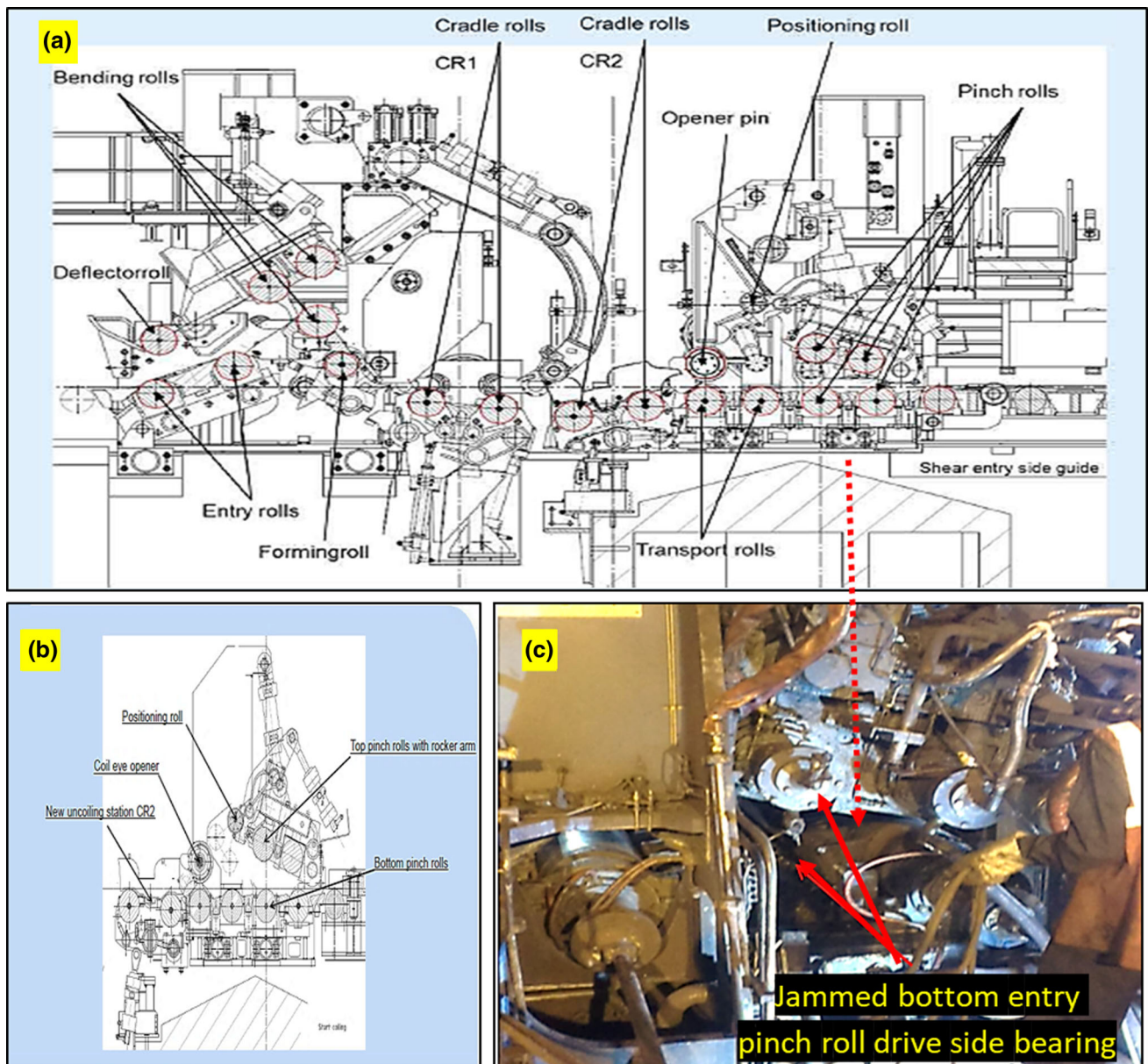


Fig. 2 Location of failure: (a) schematic showing arrangement of rolls in hot strip mill, (b) schematic of pinch rolls, (c) on-site image of location of failure

Figure 3 shows a schematic of a pinch roll bearing used in HSM. It has three major elements, namely outer ring, inner ring and barrel-shaped rollers. There are two sets of rollers partitioned by a separator as shown in Fig. 3. The mechanism of operation of the bearing is such that rollers roll around the inner race like a car wheel, but traverse around the circumference much slower than the inner race. The outer ring is stationary, whereas the inner ring revolves which drives the shaft. There was an important finding during the on-site observation. It was observed that rollers on the near end of the actual roll were broken and were found to be in severely damaged condition, whereas those located toward the near end of the shaft remained in an

undamaged state. This suggests there was a non-uniform stress distribution across the separator.

Experimental Procedure

The following methodology was used while carrying out root cause failure analysis of the pinch roll bearing:

Visual Observations

Observations were made with regard to the presence or absence of coloration, spalling, dent marks, brinelling,

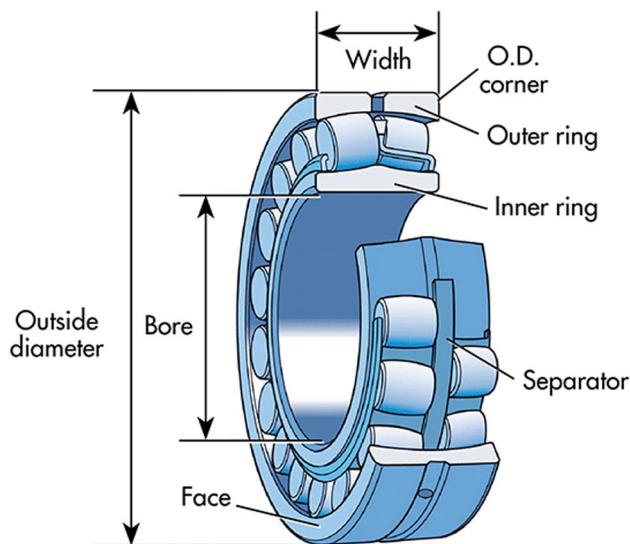


Fig. 3 Schematic of a pinch roll bearing used in HSM [7]

false-brinelling, etc. It helped to rule out a number of possible causes of failure and shifted focus to the remaining possibilities that might have led to failure. Moreover, the fracture surfaces were examined to infer primary failure mode.

SEM-Fractography

Fractography was carried out to ascertain the failure mode and observe related information for stress analysis. The fracture surface was examined under Zeiss Scanning Electron Microscope (SEM) at magnifications of $1000\times$ and $7500\times$ and accelerating voltage of 20 kV.

Lubrication Testing

Viscosity measurement was taken using a Groove Field Viscometer. A ferrography test of the lubricant was carried out to determine whether there was any foreign particle entrapment and formation of oxide debris during its operation.

Chemical Analysis

Chemical analysis was performed to determine the grade of the bearing elements and their suitability for the application. X-ray fluorescence (XRF) was used for the chemical analysis of the samples; carbon (C) and sulfur (S) contents were determined using combustion infrared technique.

Microstructural Characterization

Samples of the rollers, inner race and outer race were cut from damaged and undamaged locations using a slow disk

cutting machine. These were hot-mounted in polymeric resin, ground and polished using silicon carbide emery paper to a fineness of 2000. This was followed by cloth polishing using diamond paste of $1\ \mu\text{m}$ fineness. Final step of sample preparation was ultrasonic cleaning using acetone. Etching was carried out using nital solution (3 vol.% nitric acid in ethanol). Samples were examined in unetched condition for inclusion rating and etched condition for studying microstructural features. Microstructural examination was carried out using an optical microscope (Leica, DMRX, Germany).

SEM-EDS Analysis

Samples were examined with a Zeiss Scanning Electron Microscope (SEM). SEM-EDS analysis was performed to determine the nature of precipitates in the microstructure and to determine crack-precipitate interaction.

X-ray Diffraction (XRD) Analysis

XRD analysis was performed to determine the phases present in the bearing elements, and their phase fraction was calculated using Rietveld analysis. Copper K-alpha radiation was used in the present study. The purpose of doing so was to determine whether there is an excess retained austenite, which is difficult to quantify using microscopic techniques.

Hardness Measurements

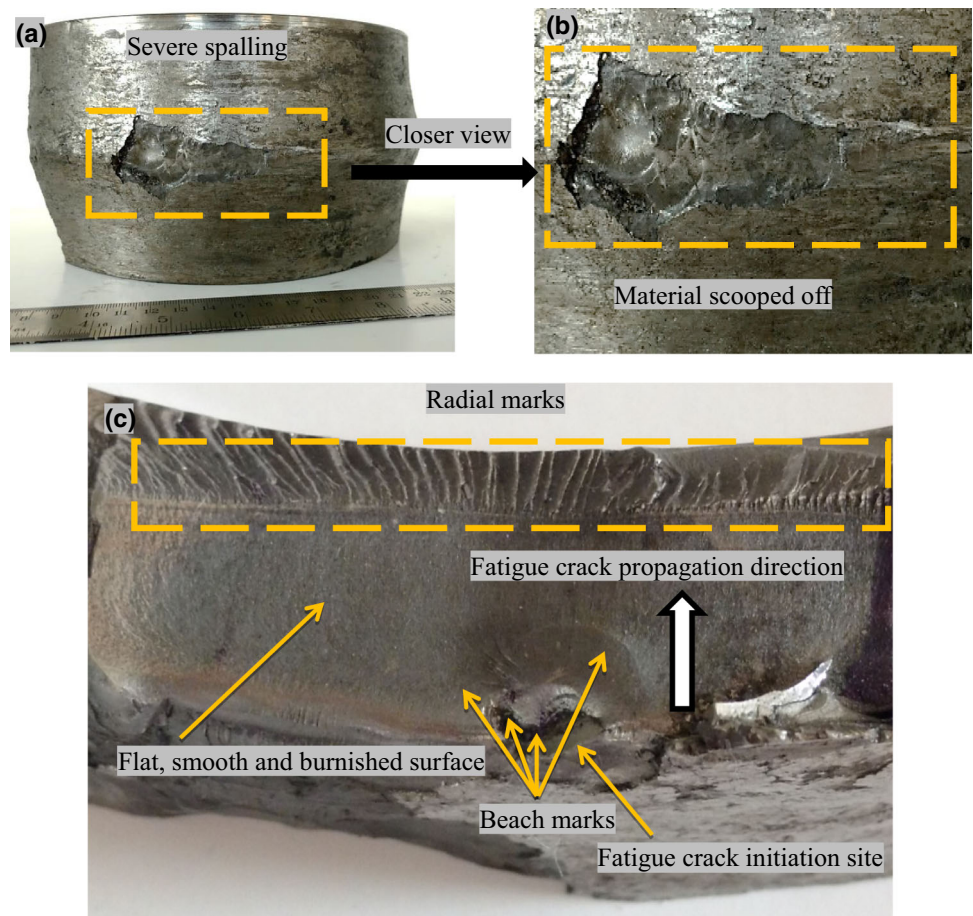
Hardness of all the bearing elements was conducted using Rockwell hardness tester on HRC scale.

Results and Discussion

Visual Observations

Since the pinch roll bearing failed and was found to be broken into multiple pieces, only those portions/pieces revealing key information regarding failure are presented in this manuscript. Figure 4 shows key aspects of failed inner ring. Figure 4a shows the outer surface of inner race which is in direct contact with the rotating rollers. It has a split mark at the center where the separator is placed and keeps two sets of rollers apart. Uniform rubbing marks were observed along the entire length of the inner race. Severe spalling was observed, and a closer view is shown in Fig. 4b. Spalling is the progressive scooping off of the material and is generally associated with rolling contact fatigue in bearings. It should be noted that there was no bluish/golden coloration, suggesting that significant

Fig. 4 Visual images of failed inner race: (a) outer surface of inner race, (b) closer view of spalling, (c) fracture surface



temperature rise did not occur during the service. Moreover, there were no pronounced dent marks or brinelling, thus ruling out contamination and sudden impact loading, respectively. No corrosion residue was observed that might accelerate fatigue.

Visual images of the failed outer race and rollers are shown in Fig. 5a and b, respectively. Figure 5a shows the fracture surface of the outer race, which exhibited beach marks on a highly smooth surface. On traversing from left to right, there is a change in contrast from darker shades to lighter shades. These features indicate fatigue mode of failure. Beyond beach marks, radial marks were observed which suggests that final fracture occurred in a brittle manner. Figure 5b shows representative samples of severely damaged and relatively undamaged rollers. It is clearly evident that those rollers located toward the near end of the shaft were virtually undamaged, whereas those present near the roll were broken and damaged to a great extent. This clearly indicates non-uniform loading was experienced by the bearing elements.

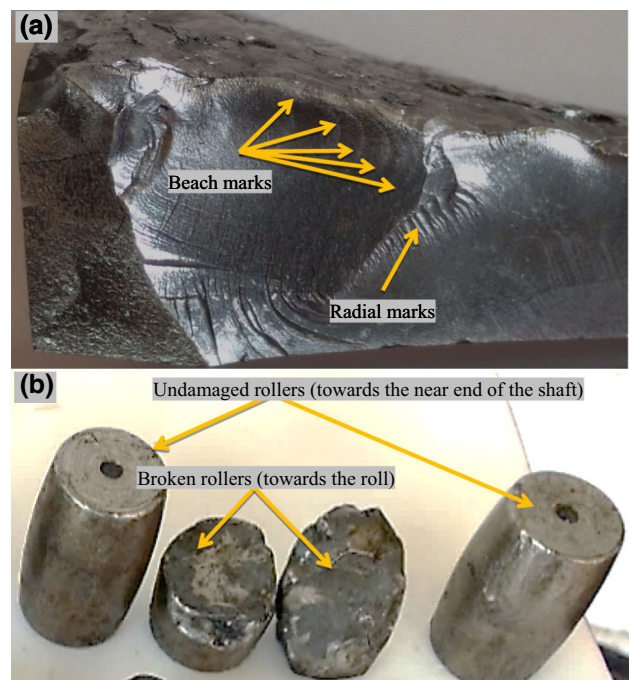


Fig. 5 Visual images showing (a) fracture surface of outer race (b) representative damaged and undamaged rollers

Fractography

Figure 6 shows SEM fractographs of the inner race which revealed striation marks confirming fatigue mode of failure. The spacing of the striation marks, i.e., distance between adjacent striation marks, indicates crack propagation at each cycle of fatigue loading (da/dN).

Lubrication Analysis

Viscosity Measurement

As per the specification, the lubricant should have viscosity close to 320 Pst. Viscosity of the used lubricant was measured to be 322 Pst, whereas that of the new lubricant was measured to be 320 Pst. This suggests that the lubricant used in pinch roll bearing met the specification, and hence, failure due to improper use of lubricant can be ruled out.

Ferrographic Analysis

Figure 7a and b shows two representative ferrograms of the lubricant used in the pinch roll bearing system. Bearing debris is flat and laminar. Such chunky debris is associated with severe subsurface fatigue. In general, chunky debris with high aspect ratio indicates an advanced stage of

fatigue [8]. Moreover, no dark oxides were observed indicating that there was no abnormal rise in temperature of the lubricant during service and the bearing operated under rated speed. In addition, there was no trace of contaminants or corrosive particles precluding premature failure due to contamination or corrosion, respectively.

Chemical Analysis

Chemical analysis of the bearing elements is summarized in Table 1.

Although the exact grade of the bearing elements was unknown, chemistry closely matched with ASTM A-485-03 (Grade 1) steel which is an anti-friction bearing grade. It is important to carry out oxygen analysis, since an increase in oxygen content of the bearing steel will manifest as an increase in inclusion size, which in turn exponentially decreases its fatigue life [9]. Oxygen content of all the bearing elements was quite low. Overall, chemical analysis suggests that steel used was suitable for the application from point of view of its chemistry.

Microstructural Analysis

Optical micrographs of the outer surface of the inner race which is in direct contact with the rotating rollers are shown in Fig. 8. Figure 8a, b and c shows unetched

Fig. 6 SEM fractographs of inner race at: (a) $\times 2500$ and (b) $\times 7500$

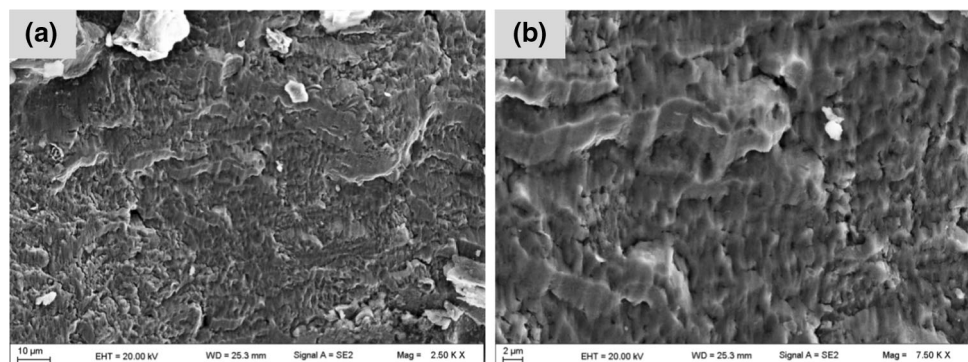


Fig. 7 Ferrograms showing two different types of low-alloy wear particles at $\times 500$

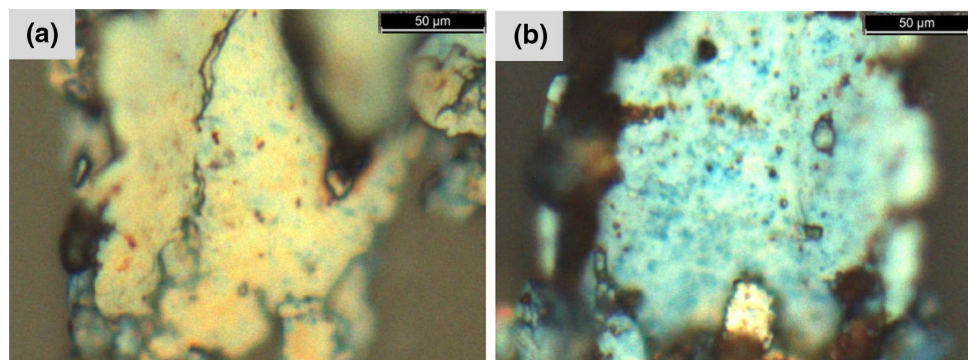
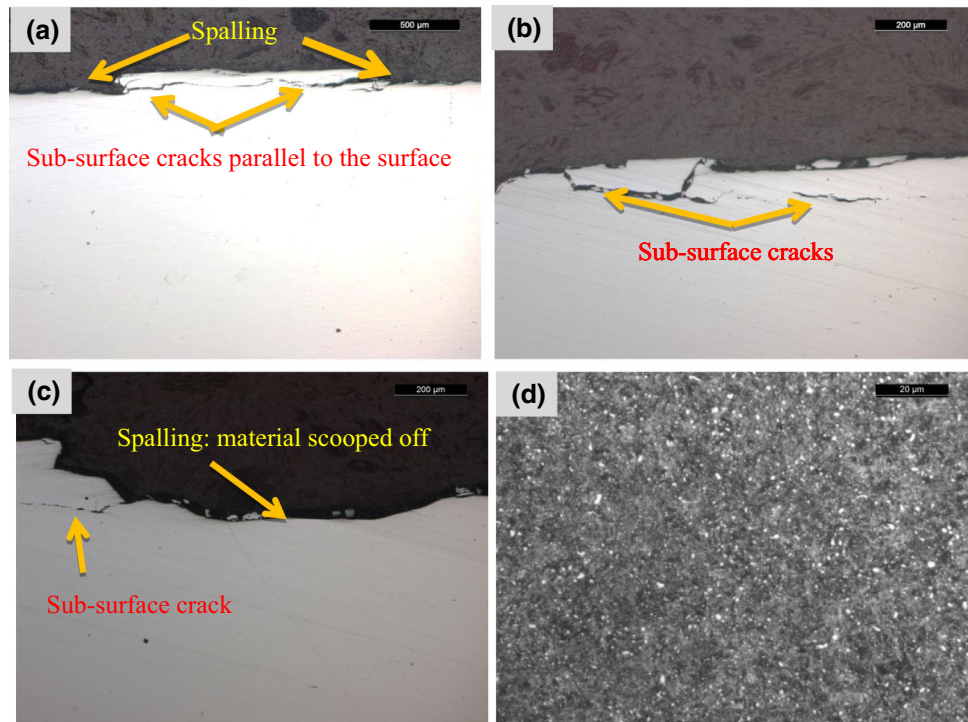


Table 1 Chemical analysis (wt.%) of bearing elements

Bearing element	C	Mn	Si	S	P	Cr	Ni	Mo	O
Inner race	0.98	1.08	0.61	0.015	0.017	1.06	0.08	0.02	4 ppm
Outer race	1.04	1.2	0.51	0.010	0.011	1.15	0.06	0.01	7 ppm
Roller	0.99	1.08	0.60	0.011	0.019	1.07	0.06	0.02	4 ppm
ASTM A-485-03 (Grade 1)	0.90–1.05	1.05–1.20	0.45–0.75	0.015 Max	0.015 Max	0.90–1.20	0.25 Max	0.1 Max	...

Fig. 8 Optical micrographs of failed inner race: (a) unetched micrograph at location 1, (b) unetched micrograph at location 2, (c) unetched micrograph at location 1- \times 100, (d) etched micrograph- \times 1000

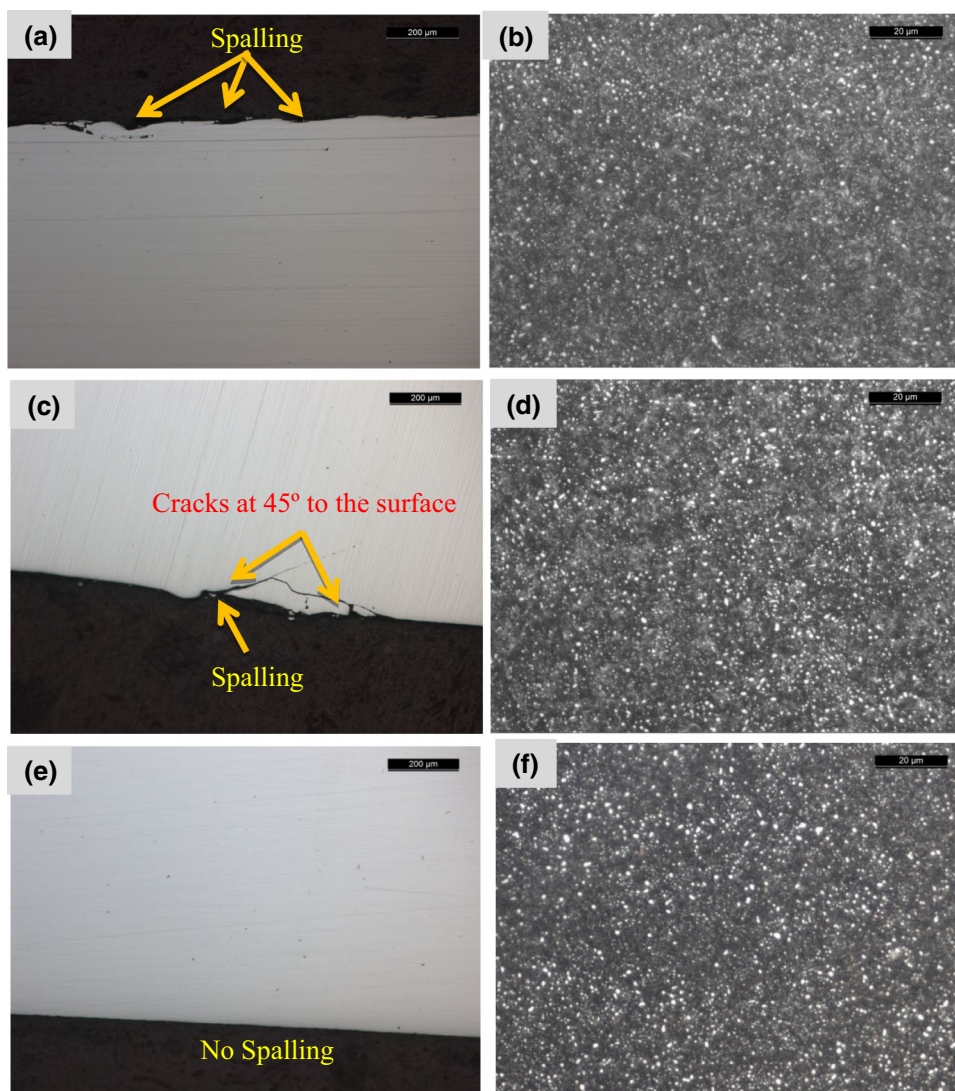


micrographs of inner race at different locations and magnifications. Subsurface cracks parallel to the rolling contact surface were observed and are shown in Fig. 8a and b. Figure 8c shows scooping off of material up to a depth greater than 250 μ m. Such localized scooping off of material from the surface is termed “spalling” and is associated with conventional rolling contact fatigue. Etched micrograph of the inner race shown in Fig. 8d revealed tempered martensitic structure with uniform distribution of carbide precipitates. Such a microstructure is desirable for bearing application.

The outer race exhibited a spalled surface and cracks parallel to the contact surface as shown in Fig. 9a. Figure 9c shows the unetched micrograph of a damaged roller located on the right side of the separator. It also has a

spalled surface, though in this case cracks were observed to be at an angle of approximately 45° to the contact surface. Such geometries of surface cracks have been reported in the literature and are associated with rolling contact fatigue. Contrary to the spalled surface of the rollers on the right side of the separator, those on the left side of the separator showed a completely undamaged surface as shown in Fig. 9e. Presence of inclusions can initiate fatigue crack; however, no ratable inclusions were observed in any of the bearing elements. This confirms that the steels used for the manufacturing of the bearing elements are clean, ruling out premature failure due to improper secondary steel making process. Etched micrographs of outer race, damaged roller and undamaged roller are shown in Fig. 9b, d and f, respectively. They show typical microstructure of

Fig. 9 Optical micrographs showing: (a) unetched outer race- $\times 100$, (b) etched outer race- $\times 1000$, (c) unetched damaged roller- $\times 100$, (d) etched damaged roller- $\times 1000$, (e) unetched undamaged roller- $\times 100$, (f) etched undamaged roller- $\times 1000$



bearing with fine distribution of carbides in the matrix. However, at $1000\times$ magnification, the microstructure of matrix is not properly resolved and this has been analyzed in detail in the following sections.

SEM–EDS Analysis

SEM–EDS analysis was performed to resolve the matrix phase, to determine the crack propagation path and to ascertain the nature and distribution of precipitates. Figure 10a shows a SEM micrograph of the spalled inner race. It revealed two nearly parallel subsurface cracks and a secondary crack perpendicular to the surface. A high-magnification micrograph ($5000\times$) near spalled surface is shown in Fig. 10b. It shows crack–precipitate interaction. Cracks tend to propagate around the precipitates rather than

cutting through them. This was confirmed by EDS point scans as shown in Fig. 10b and depicted in Table 2.

Moreover, sharp martensitic laths were not observed near the spalled region, suggesting local tempering during the process there. Figure 10c shows a micrograph of the inner race away from the spalled location. It revealed sharp martensitic lath with a uniform distribution of fine chromium carbide precipitates. This indicates that the microstructure of the bearing elements was as per requirement, though minor deterioration occurred by tempering in the vicinity of the spalled region.

XRD Analysis

X-ray diffraction was carried out for the inner race, damaged and undamaged rollers. Phase fraction of martensite

Fig. 10 SEM Micrographs of spalled inner race at (a) $\times 1000$, (b) $\times 5000$: near spalled surface, (c) $\times 5000$: away from spalled surface

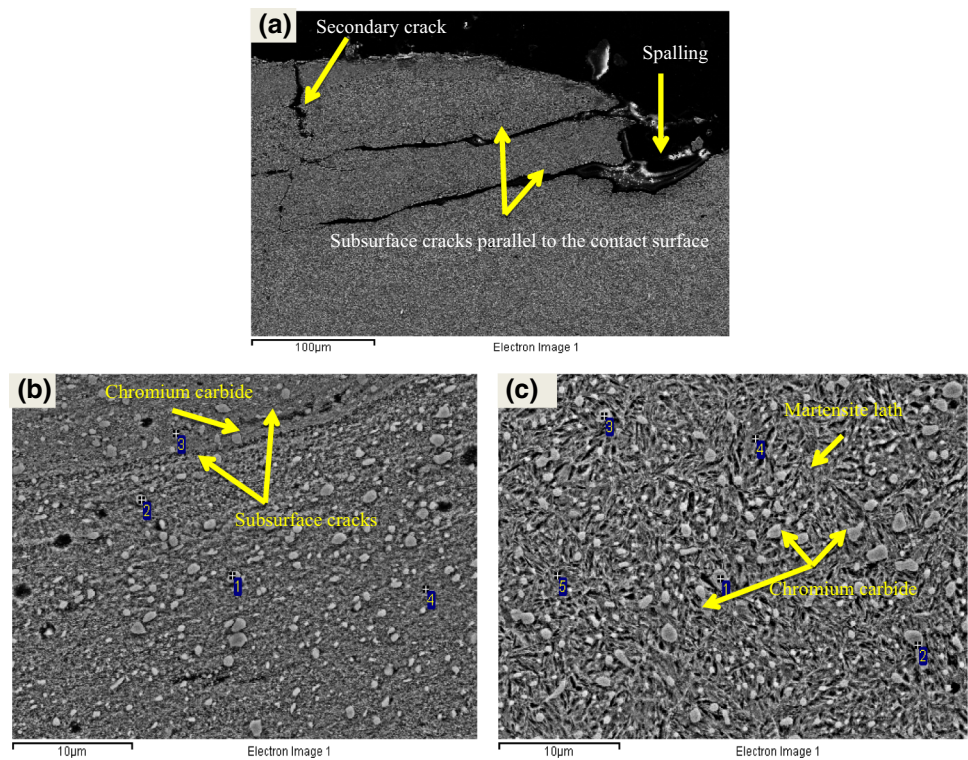


Table 2 EDS Point analysis near spalled region of inner race

Spectrum	C	Cr	Mn	Fe
1	28.36	5.24	2.68	63.72
2	29.12	3.73	2.34	64.81
3	22.11	0.63	...	77.26
4	29.75	0.88	...	69.37

and retained austenite was calculated for each case. Intensity versus 2θ plot for the inner race and rollers is shown in Fig. 11a and b, respectively. Using Rietveld analysis, it was calculated that the fraction of martensite and retained austenite was approximately 93 and 7%, respectively, in inner race. Moreover, percentage of retained austenite was close to 10% in both damaged and undamaged rollers. An excess of retained austenite is known to have an adverse effect on dimensional stability of the material. However, up to 10% of retained austenite may

not have marked effect on the dimensional stability and failure of the bearings [1].

Hardness Measurements

Rolling contact fatigue life of bearings is strongly dependent on their hardness [3]. Table 3 summarizes hardness results of different elements of pinch roll bearing. Bulk hardness of the bearing elements was within the specification. Although a hardness of 60-62 HRC would have improved its fatigue life, a marginally lower hardness cannot be the root cause of premature failure. This is because there was damage to rollers on only one side of the separator despite the fact that hardness of rollers on either side was the same. However, for life cycle improvement, higher hardness bearing steel is recommended. This can be achieved by increasing chromium content to around 1.5% which in turn will increase the volume fraction of chromium carbide precipitates.

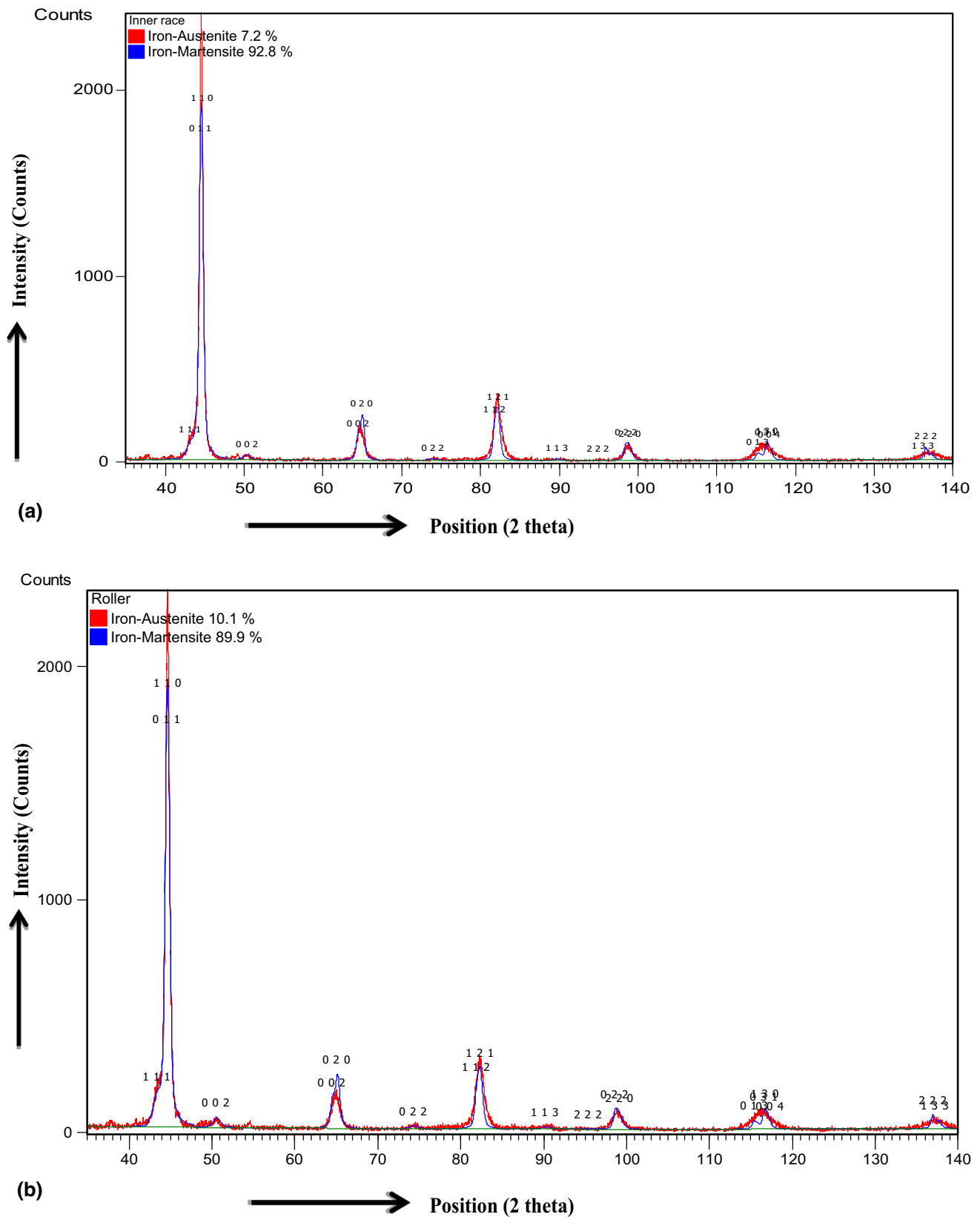


Fig. 11 XRD (Intensity vs. 2θ) plot for (a) inner race; (b) roller

Table 3 Hardness values of different bearing elements

Bearing element	Average hardness (HRC)
Inner race	59
Outer race	59.4
Damaged rollers	59.3
Undamaged rollers	59.3

Conclusion

Pinch roll bearing failed prematurely in “rolling contact fatigue” mode as suggested by beach marks and fatigue striations due to misalignment.

Recommendations

1. Source of misalignment should be identified during shut down.
2. Thermal imaging for in situ detection of misalignment can be used to prevent catastrophic failures of bearings.

Acknowledgments Authors are grateful to Tata Steel Limited, Jamshedpur, for the financial support to carry out this work. Authors express their sincere thanks to Dheeraj Kumar Lal, Susovan Das and Vikram Sharma for support in investigation.

References

1. H.K.D.H. Bhadeshia, Steels for bearings. *Prog. Mater. Sci.* **57**, 268–435 (2012)
2. A.B. Jones, *Symposium on Testing of Bearings* (American Society for Testing and Materials, Philadelphia, 1947), pp. 35–52
3. E.V. Zeretsky et al., *Effect of component differential hardness on rolling-contact fatigue and load capacity*, NASA TN D-2640 (National Aeronautics and Space Administration, Washington, DC, 1965)
4. F. Masi et al., Coupling system dynamics and contact behaviour: Modelling bearings subjected to environmental induced vibrations and ‘false brinelling’ degradation. *Mech. Syst. Signal Process.* **24**, 1068–1080 (2010)
5. Z. Chang et al., Main failure mode of oil-air lubricated rolling bearing installed in high speed machining. *Tribol. Int.* **112**, 68–74 (2017)
6. T.A. Harris, M.N. Kotzalas, *Rolling Bearing Analysis-Advanced Concepts of Bearing Technology*, 5th edn. (Taylor & Francis Group, London, 2006)
7. <http://www.machinedesign.com>
8. W.R. Jones, S.H. Loewenthal, in *Ferrographic Analysis of Wear Debris From Full Scale Bearing Fatigue Tests*, NASA Technical Paper (1979)
9. J. Monnot, et al., in *Relationship of Melting Practice, Inclusion Type, and Size with Fatigue Resistance of Bearing Steels. Effect of Steel Manufacturing Process on the Quality of Bearing Steels*, ASTM STP 987, J.J.C. Hoo (ASTM, Philadelphia, 1988), pp. 149–165

Publisher’s Note Springer Nature remains neutral with regard to jurisdictional claims in published maps and institutional affiliations.